

Long-Horizon Traffic Forecasting via Incident-Aware Conformal Spatio-Temporal Transformers

Mayur Patil¹, Qadeer Ahmed¹, Shawn Midlam-Mohler¹, Stephanie Marik², Allen Sheldon³, Rajeev Chhajer³, Nithin Santhanam³

Abstract—Reliable multi-horizon traffic forecasting is challenging because network conditions are stochastic, incident disruptions are intermittent, and effective spatial dependencies vary across time-of-day patterns. This study is conducted on the Ohio Department of Transportation (ODOT) traffic count data and corresponding ODOT crash records. This work utilizes a Spatio-Temporal Transformer (STT) model with Adaptive Conformal Prediction (ACP) to produce multi-horizon forecasts with calibrated uncertainty. We propose a piecewise Coefficient of Variation (CV) strategy that models hour-to-hour travel-time variability using a log-normal distribution, enabling the construction of a per-hour dynamic adjacency matrix. We further perturb edge weights using incident-related severity signals derived from the ODOT crash dataset that comprises incident clearance time, weather conditions, speed violations, work zones, and roadway functional class, to capture localized disruptions and peak/off-peak transitions. This dynamic graph construction replaces a fixed-CV assumption and better represents changing traffic conditions within the forecast window. For validation, we generate extended trips via multi-hour loop runs on the Columbus, Ohio, network in SUMO simulations and apply a Monte Carlo simulation to obtain travel-time distributions for a Vehicle Under Test (VUT). Experiments demonstrate improved long-horizon accuracy and well-calibrated prediction intervals compared to other baseline methods.

Index Terms—Traffic flow prediction, adaptive adjacency matrices, spatio-temporal transformer, uncertainty quantification

I. INTRODUCTION

URBAN traffic networks operate under continual incidental changes such as ever-changing weather, road constructions, breakdowns, crashes, special events, and heterogeneous driver behaviors. Due to these variables, forecasting models must adapt to changes that can occur within short time periods throughout the day. According to the 2024 INRIX Global Traffic Scorecard [1], an average driver in the U.S. spends about 43 hours stuck in traffic, resulting in an estimated loss of \$771 in time for each driver. New York and Chicago ranked the highest, with drivers in those cities losing 102 hours each, highlighting the severity of the issue. At the same time, roadway safety remains a major concern; the

most recent national crash totals are reported for 2023 (6.14 million police-reported crashes, 40,901 fatalities, and about 2.44 million injuries) [2]. Full-year crash totals for 2024 are not yet finalized; however, NHTSA’s early estimates indicate that about 39,345 people died in motor vehicle traffic crashes in 2024 [3]. These numbers motivate predictive models that are aware of incident-driven disruptions in traffic operations, beyond recurrent congestion patterns. Weather further complicates operations by amplifying delays and risks during peak periods. Federal guidance indicates that adverse weather is the second-largest source of non-recurrent congestion, where even light rain can inflate travel-time delays by 12-20% [4]. The practical need is clear: agencies and mobility providers require reliable, long-horizon forecasts with calibrated confidence to plan operations under variability and disruptions.

From a modeling standpoint, long-horizon/multi-hour traffic forecasting has always been a challenge as traffic in itself evolves throughout the day (off-peak to peak hour and back). Furthermore, exogenous factors such as roadway incidents, weather, and construction work disrupt traffic flow patterns. Conventional sequence models, such as recurrent neural networks (RNNs), are capable of handling temporal features, but they often run into issues with error accumulation and have less freedom to perform parallel processing over longer time periods. While the transformer-based designs use a self-attention mechanism to find long-range temporal relationships, and can be adjusted to include spatial relationships. Recent developments in transportation applications show that the attention-based approach can improve multi-hour accuracy and is capable of error stabilization by explicitly learning which time steps and locations matter most as the horizon extends [5]–[7].

The purpose of leveraging a transformer model for long-horizon forecasting is to look far back in history without encountering the vanishing gradient problem. This provides an adaptable mechanism to share the information spatially and scale it efficiently using parallel attention. Simultaneously, long-horizon accuracy significantly depends on how the spatial dependencies are represented, as the information of the locations can vary with time-of-day variability and disruptions caused by exogenous incidents.

In our earlier work [8], we leveraged a Graph Attention Network with Long-Short Term Memory (GAT-LSTM) with Adaptive Conformal Prediction (ACP), constructing the spatial adjacency matrix A_{ij} from a log-normal distribution repre-

arXiv:2603.16857v1 [cs.LG] 17 Mar 2026

¹Mayur Patil, Qadeer Ahmed, and Shawn Midlam-Mohler are with the Department of Mechanical and Aerospace Engineering and the Center for Automotive Research, The Ohio State University (e-mail: patil.151@osu.edu; ahmed.358@osu.edu; midlam-mohler.1@osu.edu).

²Stephanie Marik is with the Ohio Department of Transportation

³Allen Sheldon, Rajeev Chhajer, and Nithin Santhanam are with Honda Research Institute USA, Inc.

senting travel-time information. The log-normal distribution are widely used to represent travel-time stochasticity and has been reported to fit observed travel times across operating regimes in both roadway and transit settings [9], [10]. We parameterized the distribution using a fixed coefficient of variation (CV) by taking random values of travel-time to make A_{ij} dynamic in nature. Basically, it governed the dispersion of sampled travel times that we mapped onto the edge weights of GAT, and the same graph effectively governed all hours as shown in Figure 1 a. Although practically on average, the fixed-CV assumption implicitly treats the network’s variability as time-invariant.

In this work, we replace the “fixed-CV” assumption with a piecewise design by estimating an hour-of-day CV profile $CV(h)$ from historical traffic flow data (higher CV represents peak times, while lower CV represents off-peak/shoulder times). The intent is to sample log-normal edge travel times for each hour h using $CV(h)$, then introduce an incident-aware perturbation using a crash-derived severity signal calculated using incident clearance time, weather factors, speed-violation, work zones, and roadway functional class. To set up the correlation scale, we estimate edge-wise correlations between the sampled travel-time and the crash-derived attributes. We then modulate the adjusted travel times into hour-conditioned adjacency weights $A_{ij}(h)$ through a decaying kernel and normalization. This $A_{ij}(h)$ is then a set of 24-hour-conditioned graphs $A_{ij}(h)$ being fed to the model, where each training window carries its hour tag and applies the corresponding graph as visualized in Figure 1 b. To quantify uncertainty in our predictions, we retain the ACP methodology, leveraging the conformal calibration core to provide reliable confidence bounds.

To accomplish this task, we adopt a Spatio-Temporal Transformer (STT) architecture for efficient, parallel sequence modeling and integrate hour-conditioned graph derived from the proposed hour-conditioned adjacency matrices. The contributions of this paper are as follows:

- We consider an hourly CV profile from historical traffic flow data, where each hour’s CV parameterizes a log-normal distribution sample of travel times. This yields a set of hour-conditioned adjacency matrices $A_{ij}(h)$ for multi-hour forecasting.
- We introduce crash-aware perturbations of edge weights using incident-related severity signals derived from a crash dataset (incident clearance, weather factors, work zone areas, speed violations, and roadway functional class), enabling localized disruption sensitivity in the dynamic graph.
- We retain ACP for finite-sample coverage guarantees on forecasts, yielding reliable confidence around forecasted values.
- We run multi-hour SUMO simulations via Monte Carlo sampling for a Vehicle-Under-Test (VUT) trajectory and validate it against INRIX travel-time data.

The rest of the paper is organized as follows: Section II summarizes prior work on traffic flow forecasting. Section III presents the proposed framework and methodology. Section IV

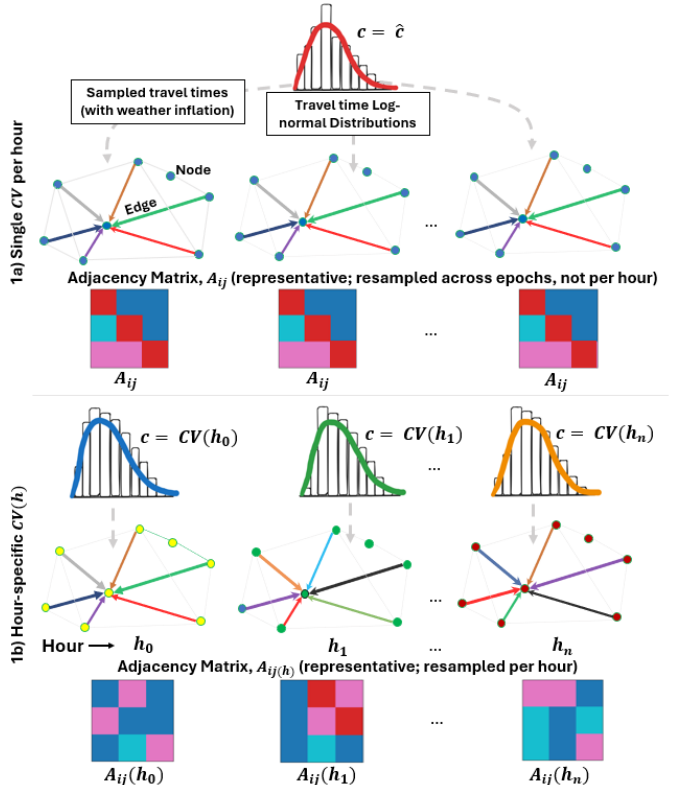


Fig. 1. Static vs. piece-wise graph priors: 1a) one fixed-CV \hat{c} drives a log-normal travel-time prior; the resulting adjacency A_{ij} is reused across hours, 1b) an hourly profile $CV(h)$ yields hour-conditioned priors and distinct adjacencies $A_{ij}(h)$. Edge colors/thicknesses are schematic.

reports the experimental setup and comparative results against baseline models. Section V concludes the paper and outlines future research directions.

II. RELATED WORK

A. Traffic Forecasting Models and Graph Learning

In the past, traffic forecasting was conducted using conventional univariate and multivariate time-series models that considered each sensor stream independently. Because of its simplicity and interpretability, the original Box-Jenkins family of AutoRegressive Integrated Moving Averages (ARIMA) continues to be a typical baseline for short-term forecasting [11]. Similarly, exponential-smoothing methods such as Simple Exponential Smoothing (SES) [12], Holt’s linear trend method [13], Holt-Winters seasonality [14], and Error Trend-Seasonality (ETS) state-space models [15] are other short-term traffic speed/flow prediction [16]. However, these approaches are only limited to short-horizon prediction as their linear dynamics struggle with nonlinear congestion patterns, they do not have encoding for spatial interactions, and their mechanism is restrictive to handle disruptions such as road incidents, demand surges, weather, etc.

However, the field made a significant impact when deep sequence models were introduced. They were shown to be capable of learning nonlinear dynamics inherently from the data. The early stacked feedforward and autoencoder-based models showed good performance for short-term traffic forecasting

[17]. Recurrent neural networks (RNNs) like LSTM/GRU variants improved multi-step prediction by maintaining temporal state and reducing the vanishing gradients problem compared to vanilla RNNs [18], [19]. Long-horizon scenarios, however, may result in the accumulation of error due to repeated rollouts, and unless explicitly introduced by design, spatial relationships remain implicit.

The bottleneck for long-horizon forecasting is that the model has to decide “what to remember” from the history and “how to roll forward” without “losing attention”. First and foremost, many temporal modeling approaches were proposed specifically to reduce this distraction. For instance, Seq2Seq encoder-decoder models addressed this problem by separating historical encoding from future decoding, so that the forecasting depends on a concise representation of the historical data and have an option to attend back to it when needed. Similarly, convolution-based approaches like LSTNet combines temporal convolutions and can skip certain connections to capture important patterns at [20], whereas Temporal Convolution Network (TCN) use dilated causal convolutions to model long-horizon aspects without distinct recurrent states [21]. Furthermore, attention-augmented recurrent models like dual-stage attention-based recurrent neural network (DA-RNN) modify the weights based on the current context, hence handling the off-peak and peak condition changes [22]. Secondly, the spatio-temporal forecasting models improved when they coupled the temporal model with an explicit graph-based framework to share information spatially. The key idea is that the model should be able to pass messages between correlated road segments rather than expecting the temporal module to infer spatial relationships. The early baselines implemented this by integrating temporal module with graph convolutions on a graph prior. For instance, STGCN fuses temporal convolutions with graph convolutions to capture general space-time relationships [23]. Then, DCRNN approach proposed a diffusion process on a directed graph and proposed a gated recurrence to modify node states over time [24], while T-GCN approach similarly integrates convolution-based spatial integration with gated temporal dynamics [25]. Furthermore, an attention-based extension was put forth by ASTGCN model which relaxed rigid neighborhood influence by learning spatial-temporal important events, thus capturing periodic information (hourly/daily/weekly) and heterogeneous node impacts [26]. Beyond these common baselines, many variants refines the temporal module, graph structure, or both. For example, traffic graph convolutional recurrent designs bolster the prediction framework by explicitly communicating information along the graph edges rather than over-utilizing the temporal module to re-learn spatial information from scratch [27].

Another advancement was made, and spatio-temporal GNNs were matured in terms of introducing dynamics in creating the adjacency matrix. Methods were proposed to make a shift from a static distance-based adjacency matrix to a more adaptive adjacency that is learned from data. Graph WaveNet introduced a data-driven spatial module and created the adjacency matrix alongside dilated causal convolutions, greatly reducing error accumulation across multi-step hori-

zons in the case of incomplete/misspecified sensor information [28]. Other models, such as GMAN used an encoder-decoder attention architecture to learn when and where to accumulate the information, while replacing the custom-built diffusion layer with learned spatio-temporal aggregation [29]. A parallel line of work studied explicitly dynamic graphs, e.g., dynamic graph convolution formulations for multi-step traffic forecasting [30], multi-weight graph architecture that put together multiple information types [31], and graph-learning STGCN variants that utilized the adjacency matrix as part of training data [32]. Other work emphasized on fusing various features/attributes, where multiple other factors of the network state were integrated instead relying on a single traffic attribute to improve robustness under dynamic operating conditions [33]. Interestingly, meta-learning has also been explored to improve transferability across the network, e.g., spatio-temporal meta-learning frameworks being capable of generalizing under distribution shifts [34], and multivariate time-series graph forecasting models such as MTGNN proposed on learning graph-structure and message passing specific to high-dimensional correlated series [35].

Despite significant progress, most of the above studies frequently considered short-horizon forecasting (typically 15-60 minutes) and/or under very smooth connectivity assumptions. On the other hand, multi-hour forecasting (e.g., predicting 2, 4, 8, or 12 hours ahead) is harder because the spatial influence pattern is not time-invariant across the day as there is peak build-up, peak dissipation, and localized disruptions that affect which links dominate the changes. This is precisely the gap we target and prioritize multi-hour forecasting by providing an hour-conditioned, variability-aware spatial information instead of a single static graph, so that long-horizon performance is not driven purely by extrapolation from a stationary connectivity assumption.

B. Long-horizon forecasting

Only a small but rising number of papers worked on the long-horizon forecasting problem. An interesting Graph Pyramid Autoformer family (X-GPA/GPA) was proposed to explicitly evaluate multi-hour settings (e.g., 2/4/8/12 hours). To focus on long-range shift stabilization, an autocorrelation-based attention approach was utilized with a pyramidal multi-scale temporal representation [36], [37]. Similarly, long-term graph learning studies also worked in the same avenue and support the claim that extending forecasting horizon beyond several hours requires stronger inductive bias to prevent model drift, including formulations that explicitly evaluate long-range prediction on graphs [38], [39].

The latest works push the design capability and extend the prediction horizons. One such model, TrafFormer, specifically defines the task of predicting traffic up to 24 hours using a Transformer framework tailored for handling long-term sequences [40]. Another model, HUTFormer, similarly does long-term forecasting beyond 1-hour and discusses the outlook on up to 1 day by leveraging hierarchical multi-scale representations to handle long input/output horizons comprehensively [41]. Additionally, system-oriented work such as Foresight

Plus focuses on establishing spatio-temporal traffic forecasting in a serverless scenario. Also, it discusses practical approaches for running the latest long-horizon models in a production pipeline [42].

Another approach uses common traffic baselines to assess robustness in multi-hour regimes explicitly. Using roughly 2-hour and 4-hour prediction settings on 5-minute datasets (e.g., PEMS-BAY), SpikeSTAG reports long-horizon results, emphasizing that multi-hour horizons reveal vulnerabilities in short-horizon-tuned architectures and that performance gains are frequently linked to maintaining cross-node propagation structure as the horizon expands [43]. Lastly, a GAT-Informer model was proposed that leverages a Transformer-like long-term forecasting module with graph attention and an Informer-like temporal modeling to perform tests at long horizons (e.g., up to 2 hours on a 15-minute dataset) [44].

C. Transformer Architectures for Traffic Forecasting

An astounding innovation of self-attention was recently developed, and it took over the artificial intelligence field with incredible results. This was the wave of Transformers, which showed that instead of relying on recurrent cells or fixed-receptive-field convolutions, the architecture was built on the standard Transformer design [45] and uses multi-head attention to connect distant time steps and locations in a single layer. Hence, making them especially attractive for multi-hour horizons and highly non-stationary urban regimes.

A Traffic Transformer approach [46] was one of the first traffic-specific Transformer designs, which extensively used the continuity and periodicity of traffic time series. The architecture simultaneously models spatial correlations between the traffic stations and incorporates temporal aspects into an encoder module. Large-scale urban dataset experiments clearly outperform RNN/CNN baselines, especially when long-range periodic patterns are critical. On the same lines, Spatio-Temporal Transformer Networks (STTN) model was proposed, which decoupled spatial and temporal modules into a separate Transformer module that handled various traffic sensor graphs [47]. Here, the spatial module captures dynamic multi-head dependencies between the nodes, and the temporal module handles the long-range time-series history. This encoder-decoder design showed significant state-of-the-art performance on the widely used PeMS dataset, particularly at long horizons where small temporal modules and static graphs showed inadequate performance.

A dynamic, hierarchical spatial-temporal Transformer formulation was also proposed [48], by stacking Transformer blocks with hierarchical attention patterns to capture short-term interactions (local) and long-term congestion (global) evolution simultaneously. The outcome was an architecture that outperforms STGCN/DCRNN baselines on multi-step traffic speed prediction and also provided interpretable attention maps showing roads and time periods influencing the performance. A bidirectional spatial-temporal adaptive Transformer (Bi-STAT) was later proposed by applying self-attention in both forward and backward temporal directions. Interestingly, they made the spatial attention pattern completely adaptive instead of a fixed adjacency matrix [49]. This

particularly raised interest in terms of how and why integration of incidents, lane closures, and other regime shifts that which is critical to capture real-world representation.

A number of studies focused on improving the temporal module of the Transformer architecture for traffic flow prediction. Specifically for traffic flow states, a Transformer-based deep neural network was proposed that enhanced the fundamental self-attention process, enhancing embedding and decoder structure [50]. To better capture complex spatio-temporal correlations while maintaining efficiency, a Fast Pure Transformer Network (FPTN) was proposed that used sequential traffic data and introduced multiple embeddings for sensor position, and temporal/positional aspects [51]. An improved version of Transformer for traffic flow prediction was later proposed by modifying input embedding and temporal attention by explicitly modeling both long-range and short-range dependencies [52]. Then, a Transformer-based short-term traffic forecasting model was introduced that systematically compared attention-based designs with conventional deep networks, while confirming that self-attention can produce more stable performance across different congestion levels and short horizons [53].

Transformers and graph-based spatial modeling are closely integrated in one of the other studies [54], introducing a spatial-temporal Transformer network that improves the traffic flow prediction using a pre-trained language model; introducing contextual information using Transformer blocks along with spatio-temporal inputs. A spatial-temporal Transformer-based traffic flow prediction model, ST-TransNet, was another distinct model for bridge networks, which jointly encodes correlations among bridges and temporal dynamics using stacked self-attention layers [55]. Furthermore, a graph-enhanced spatio-temporal Transformer was introduced that integrated graph convolutions with a Transformer layer to learn spatial representations and attention-based temporal modeling [56]. Another approach took this further by separating graph-based spatial encoding and Transformer-based temporal encoding, and then combining them again [57]. During the same time, a hybrid model was proposed that incorporated a spatio-temporal Transformer with graph convolutional networks (GCNs), exhibiting that joint attentions are much better in capturing regional interactions along with temporal dependencies [58]. As multiple works are being done following the Transformer-based approach, the Transformer-Enhanced Adaptive Graph Convolutional Network (TEA-GCN) was introduced, where Transformer modules enhance the adaptive graph learning, allowing the spatial framework to be refined in a data-driven way during training [59]. At a more comprehensive scale, a learnable long-range graph Transformer (LLGformer) was published that improved traditional Transformer-style models with techniques intended for more efficient learning of long-horizon dependencies in traffic flow data on large graphs [60].

In the above studies, we found three common points: i) Multi-head self-attention temporally offers a flexible mechanism to extract longer/multi-scale histories, reducing the vanishing gradient problem and the limiting long-range training difficulties of RNNs and TCNs, ii) To allow cross-link effects to change with time and traffic conditions rather than being

fixed by a static graph, many topologies changed from fixed, hand-crafted adjacency matrices to data-driven or adaptive spatial attention, and iii) In multi-step rollouts, encoder-decoder designs and partially parallel decoding techniques reduce exposure bias and error accumulation. However, the majority of the current works still consider the spatial structures relatively slowly varying, and they rarely encode variability caused by exogenous factors directly into the spatial module. In this work, we leverage the Transformer-based framework but fuse the encoder–decoder architecture with a variability-aware, piecewise, hour-conditioned graph derived from coefficient of variation choices. By injecting this connectivity into the Transformer architecture, the model has stochasticity available from the adaptive adjacency matrix purely from a data-driven source.

D. Incident context features

Non-recurrent congestion caused by crashes is a notable source of forecasting error whether it’s short-term or long-term. Its consequences are majorly dependent on factors like the crash/incident clearance time, weather/road condition at the time of crash, the type of roadway (functional class), construction or work-zone disruption, speed infractions, so on and so forth [61]. As crash incident response and recovery time can last from minutes to hours, the effects are especially appropriate for multi-hour horizons where the traffic states can transition from off-peak to peak hours to disrupted conditions in a single forecast window.

As a result, a substantial amount of research directly predicts the event dynamics, mostly through the prediction of incident length. The statistical learning and machine learning techniques such as hazard models, tree-based models, mixture models, and deep learning architectures can predict the length of the events and quantify the impact of other related factors as shown by some latest studies and review works [62]–[64]. These studies repeatedly emphasize that characteristics that control how disruptions develop, such as response situations and clearance-related variables, that influence incident impacts in addition to the event itself. This body of research encourages handling incident-related data as a prime signal rather than a rare incident that a general forecasting model should automatically consider.

Simultaneously, rich models for crash frequency, crash risk, and collision severity have been constructed by road-safety analytics. These models explicitly use exogenous descriptors, such as weather, roadway class/type, construction zones and variables related to speed. The occurrence and impact of crashes are structured in both location and time, as shown by spatio-temporal crash modeling and risk mapping [67], [68]. Weather and highway context (including road hierarchy/functional class) are among the most relevant factors for explaining the crash outcomes, according to severity-prediction studies [69]–[72]. The factors of interest are majorly speed-related as NHTSA reports that over-speeding contributed almost 29% of traffic fatalities in 2023, emphasizing why speed-violation indicators are important factors when characterizing crash severity [65]. Transportation officials have

long stressed that bad weather exacerbates both safety and mobility problems, as we pointed out that travel time is increased by 12-20% [4]. So, adverse weather is a leading contributor to non-recurrent delays.

In order to improve traffic speed prediction during disruptions, [66] employs event detection and representation learning to convert raw incident information into latent features. These factors are frequently integrated with graph-based models to capture the propagation patterns. Although these models confirm that incident factors lowers error during disruption periods, incident information is typically incorporated as an additional inputs in the form of a time-series data, or learned embeddings rather than as a coupling them explicitly with the spatial dependency structure.

In this study, we utilize crash context features with dynamic spatial structure. We employ incident clearance time, weather, speed violations, work zone areas and functional class to construct an incident-severity signal that modifies edge weights in an hour-conditioned adjacency matrix. This approach aligns with the logic found in the above studies where disruption impact depends on contextual factors, and its network influence is reflected in the effective connectivity used for prediction. By embedding this disruption signals into the spatial module itself, the forecasting model begins each window with a connectivity that is already biased towards the propagation patterns, rather than learning all such effects purely from historical time series.

E. Uncertainty Quantification

Uncertainty quantification is critical for multi-hour traffic forecasting, as uncertainty is state-dependent and increases with the horizon window. Essentially, crash-related disruptions (and their associated context, such as weather, speed-related behavior, work zone, and roadway functional class) can introduce abrupt distribution shifts that are not well represented by point forecasts alone. Consequently, systems do require calibrated confidence bounds in addition to point estimates. Earlier work in traffic forecasting has quantified uncertainty using Bayesian or approximate-Bayesian methods, quantile-based models, and resampling or ensemble strategies. Bayesian learning formulations have been applied to traffic speed prediction with uncertainty estimates [73]. Other practical approaches, such as Monte Carlo dropout [74] and deep ensembles [75], are widely used because they can utilize existing neural forecasters but at the cost of increased computation. Hence, they struggle to provide coverage guarantees under a distribution shift.

To handle the distribution shifts, Conformal prediction (CP) offers an exceptionally good performance by offering a complementary, distribution-free route by calibrating interval width from validation residuals, resulting in finite-sample coverage guarantees [76]. The CP family has conformalized quantile regression (CQR) that improves efficiency by conformalizing learned quantiles [77], then for non-stationary settings, adaptive conformal methods were developed to update calibration online to maintain coverage under drift [78], [79]. In this work, we retain an adaptive CP (ACP) style conformal calibration

layer while strengthening the base forecaster with crash-informed, time-varying graph connectivity. This pairing is adopted for incident-driven traffic where the dynamic graph reduces the misspecification during disruptions, while ACP provides reliability-controlled uncertainty intervals for the residual uncertainty.

III. PROPOSED METHODOLOGY

A. Graph Formulation and Data Availability

Following our prior formulation [8], we model the sensor network as a directed graph $\mathcal{G} = (\mathcal{V}, \mathcal{E})$ (nodes are stations; edges are feasible directed links). where we have two types of stations i) Continuous Count Stations (CCS), and ii) Non-Continuous Count Stations (N-CCS), providing traffic data in a rich (5/15 min interval; each day of the year) and sparse manner (maybe for a few days/months only), respectively. We are reiterating the approach in this work- each node i is assigned a data-availability score $a_i \in [0, 1]$:

$$a_i = \begin{cases} 1, & i \text{ is CCS} \\ \frac{C_i}{\max_j C_j}, & i \text{ is N-CCS} \end{cases} \quad (1)$$

where C_i is the count data from N-CCS node i , and $\max_j C_j$ is the maximum count observed among all N-CCS stations. Then, we modify it to an edge-wise reliability mask as:

$$\mathbf{A}_{\text{avail}}[i, j] = a_i a_j \quad (2)$$

We apply $\mathbf{A}_{\text{avail}}$ as a multiplicative mask on the learned hour-conditioned adjacency in later sections. (*Please note that \mathcal{E} is the edge notation different than $\varepsilon > 0$ which is used throughout the paper as tiny constant to avoid division by zero.*)

B. Hourly Adaptive Adjacency Matrix Formulation

Considering network variability as time-variant is one of the main objectives of this work. Practically, the spread of travel times increases significantly during peak hours and decreases during off-peak hours. To capture this effect, we construct an hour-of-day coefficient-of-variation profile:

$$\text{CV}(h) \in [0.1, 1.0], \quad h \in \{0, 1, \dots, 23\} \quad (3)$$

estimated from historical flow data. Understandably, the low traffic conditions, like late night, are represented by a small CV(h), and heavy traffic times, like morning/evening peaks, are represented by a larger CV(h). For instance, if we consider a typical case, very early-morning hours such as 03:00-05:00 AM typically fall near $\text{CV}(h) \approx 0.15$ -0.25 (free-flow with small spread), the mid-morning and early-afternoon periods around 08:00-10:00 and 13:00-14:00 rise to $\text{CV}(h) \approx 0.35$ -0.50, and the main peaks around 16:00-18:00 can reach $\text{CV}(h) \approx 0.70$ -0.90. After the evening peak, the coefficient gradually drops again, with late-night hours (21:00-01:00) returning toward $\text{CV}(h) \approx 0.20$ -0.30.

Let the baseline mean travel time between stations i and j be represented by T_{ij}^{mean} . For a given hour h , we model the stochastic travel time $T_{ij}^{(h)}$ as a log-normal distribution:

$$T_{ij}^{(h)} \sim \text{LogNormal}(\mu_{ij, \ln}^{(h)}, \sigma_{\ln}^{(h)}) \quad (4)$$

with the constraint that the distribution has mean T_{ij}^{mean} and coefficient of variation $\text{CV}(h)$. For hour-specific cases, we compute the parameters of the lognormal distribution as:

$$\sigma_{\ln}^{(h)} = \sqrt{\ln(\text{CV}(h)^2 + 1)} \quad (5)$$

$$\mu_{ij, \ln}^{(h)} = \ln(T_{ij}^{\text{mean}}) - \frac{1}{2}(\sigma_{\ln}^{(h)})^2 \quad (6)$$

We then draw samples from $T_{ij}^{(h)}$ and assemble them into an hour-specific travel-time matrix, and repeating this for all $h \in \{0, \dots, 23\}$ produces a piecewise (hour-indexed) collection of travel-time adjacency matrices:

$$\{\mathbf{T}^{(h)}\}_{h=0}^{23} \quad (7)$$

where each $\mathbf{T}^{(h)}$ is explicitly aligned with the hour's variability using $\text{CV}(h)$. This matrix collection serves as the stochastic travel-time "prior" that is later converted into hour-conditioned adjacency weights. This enables the spatial connectivity used by the model to change with the time-of-day rather than remaining fixed across the entire forecasting window.

C. Crash Attributes Integration in Adjacency Matrices

We use the crash data from the Ohio Department of Transportation (ODOT), which are then (along with their attributes) aligned in space and time with the ODOT traffic count dataset. This is done to enable their aggregation into hour-conditioned risk signals used in our adjacency construction. Each crash record n provides a location, timestamp, incident clearance time, followed by contextual attributes like weather/functional-class/work-zone code, vehicle speed, and posted speed limit. Table I summarizes the notation used throughout the paper for these attributes.

TABLE I
CRASH DATA AND NOTATIONS

Symbol	Description	Units / Type
(ϕ_n, λ_n)	latitude/longitude	degrees
t_n	timestamp	datetime
C_n	incident clearance time	minutes
ω_n	weather condition code	categorical
f_n	roadway functional class code	categorical
v_n	observed vehicle speed	mph (or km/h)
v_n^{lim}	posted speed limit	mph (or km/h)
z_n	work-zone indicator	{0, 1}

The first step is to perform the spatial mapping, because crash locations do not coincide exactly with the traffic stations. So, we associate each crash to its nearest station in \mathcal{V} :

$$\pi(n) = \arg \min_{i \in \mathcal{V}} d((\phi_n, \lambda_n), (\phi_i, \lambda_i)) \quad (8)$$

where $d(\cdot, \cdot)$ denotes a distance metric (e.g., geodesic distance or a local Euclidean approximation). We then further assign each crash to its particular hour-of-day, which aligns the crash aggregation with the hour-conditioned travel-time matrices $\{\mathbf{T}^{(h)}\}_{h=0}^{23}$ defined in Equation 7.

As our goal is not to treat each attribute as an independent factor in the adjacency matrix, but to build a single combined

severity signal that reflects how disruptive a crash can be, which is done by the following formulation:

Incident Clearance Time (ICT) factor: Let \bar{C} denote the global mean clearance time across the crash dataset. For crash n :

$$c_n = \frac{C_n}{\bar{C} + \varepsilon}. \quad (9)$$

Speed violation factor: We define a non-negative overspeed ratio as:

$$r_n = \max\left(0, \frac{v_n - v_n^{\text{lim}}}{v_n^{\text{lim}} + \varepsilon}\right) \quad (10)$$

and normalize it using the global mean \bar{r} :

$$\tilde{r}_n = \begin{cases} \frac{r_n}{\bar{r} + \varepsilon}, & \bar{r} > 0 \\ 1, & \bar{r} = 0 \end{cases} \quad (11)$$

Weather and functional-class factors: By comparing mean clearance times by category, we formulate these factors. Let $\mathbb{E}[C \mid \omega]$ be the mean clearance for weather code ω , and similarly $\mathbb{E}[C \mid f]$ for functional class f . Then we define:

$$m_{\omega_n} = \frac{\mathbb{E}[C \mid \omega_n]}{\bar{C} + \varepsilon}, \quad m_{f_n} = \frac{\mathbb{E}[C \mid f_n]}{\bar{C} + \varepsilon}. \quad (12)$$

The conditional means are computed empirically as:

$$\mathbb{E}[C \mid \omega] \approx \frac{1}{N_\omega} \sum_{n:\omega} C_n \quad (13)$$

$$\mathbb{E}[C \mid f] \approx \frac{1}{N_f} \sum_{n:f} C_n \quad (14)$$

where N_ω and N_f are the number of crashes in each weather, and functional-class groups.

Work-zone factor: The work-zone factor $z_n \in \{0, 1\}$ is integrated using:

$$m_{z_n} = \frac{\mathbb{E}[C \mid z_n]}{\bar{C} + \varepsilon}, \quad (15)$$

$$\mathbb{E}[C \mid z] \approx \frac{1}{N_z} \sum_{n:z} C_n \quad (16)$$

where N_z denote the number of crashes in work-zone group.

Eventually, we arrive at the proposed definition of crash-level combined severity as:

$$s_n = c_n \cdot \tilde{r}_n \cdot m_{\omega_n} \cdot m_{f_n} \cdot m_{z_n} \quad (17)$$

D. Hourly Crash Risk Signals

As the crash records are localized data with their associated attributes, and forecasting models usually ingest a pairwise connectivity matrix (a travel-time-based and hour-specific in our case). In order to address this, we need to first aggregate the crash influence at the node level by hour-of-day, and then project it to edge edge-level signal. This modulates the travel-time-based connectivity, as each crash record n is mapped to its nearest station $\pi(n) \in \mathcal{V}$ and has a combined severity score s_n . Now, for each hour-of-day $h \in 0, \dots, 23$, we define the node risk as the accumulated severity at station i as:

$$\mathcal{C}_{h,i} = \{n \mid \text{hour}(n) = h, \pi(n) = i\} \quad (18)$$

$$R(h, i) = \sum_{n \in \mathcal{C}_{h,i}} s_n \quad (19)$$

To make it more clear, $R(h, i)$ depicts the cumulative impact of a crash near a station i at hour h . When no crash maps to (h, i) , the risk can be $R(h, i) = 0$, meaning no additional incident affect is applied at that station-hour; this does not imply that the resulting graph connectivity becomes binary. In the subsequent adjacency construction, edge weights remain dense and continuous due to the applied travel-time kernel. Next step is to standardize $R(h, i)$ as:

$$\hat{R}(h, i) = \frac{R(h, i) - \mu_R}{\sigma_R + \varepsilon} \quad (20)$$

where μ_R and σ_R are the global mean and standard deviation of $R(h, i)$, and $\varepsilon > 0$ ensures numerical stability. Now, the subsequent graph creation builds on the station pairs (i, j) , i.e., dense $N \times N$ interactions used to form an hour-based adjacency. Therefore, we need to project the node-level signal to the pairwise matrix by summing the risks of the endpoints:

$$\hat{R}_{total}(h, i, j) = \hat{R}(h, i) + \hat{R}(h, j) \quad \forall i, j \in \mathcal{V} \quad (21)$$

The understanding here is that if the endpoint stations observe an increased severity at hour h , then the connectivity between the two stations is more likely to be affected (maybe due to localized queues propagating upstream/downstream). Technically, $\hat{R}_{total}(h, i, j)$ portrays an hour-specific ‘‘incident affect’’ situation that can be used to perturb sampled travel times before converting them into the final hour-conditioned adjacency matrix.

E. Formulating Incident-Aware Adjacency Matrix

After the formulation of $\hat{R}_{total}(h, i, j)$, we now need to establish the relation between each node pair’s (i, j) aggregated crash-context signal and sampled travel times. To accomplish this, we use Pearson correlation coefficients as:

$$\rho_{ij} = \text{Corr}_h(T_{ij}^{(h)}, \hat{R}_{total}(h, i, j)), \quad (22)$$

where $\text{Corr}_h(\cdot, \cdot)$ denotes the Pearson correlation computed over the 24 hourly samples $h = 0, \dots, 23$. And, we bound the correlation coefficient to maintain numerical stability as:

$$\rho_{ij} \leftarrow \text{clip}(\rho_{ij}, -\rho_{\max}, \rho_{\max}). \quad (23)$$

We then define the incident-aware effective travel time for hour h as:

$$\hat{T}_{ij}^{(h)} = T_{ij}^{(h)} \left(1 + \rho_{ij} \hat{R}_{total}(h, i, j)\right), \quad (i, j) \in \mathcal{E} \quad (24)$$

Finally, we convert the incident-aware travel times into hour-conditioned adjacency weights using a Gaussian kernel [23]:

$$A_{ij}^{(h)} = \exp\left(-\frac{1}{2\sigma^2} \left(\frac{\hat{T}_{ij}^{(h)}}{T_{\max}^{(h)} + \varepsilon}\right)^2\right) \quad (25)$$

$$T_{\max}^{(h)} = \max_{(u,v) \in \mathcal{E}} \hat{T}_{uv}^{(h)} \quad (26)$$

where $T_{\max}^{(h)}$ is the maximum effective travel time at hour h , and σ^2 controls how sharply connectivity decays with increasing travel time. Finally, we obtain the adaptive adjacency matrix by applying the data-availability mask $\mathbf{A}_{\text{avail}}$ defined in Equation 2 to the hour-conditioned adjacency:

$$\mathbf{A}_{\text{adaptive}}^{(h)}[i, j] = A_{ij}^{(h)} \cdot \mathbf{A}_{\text{avail}}[i, j] \quad (27)$$

This yields a collection of incident-aware, hour-conditioned adaptive adjacency matrices where each $\mathbf{A}_{\text{adaptive}}^{(h)}$ combines incident-aware travel-time perturbations (incident clearance, weather, functional class, speeding, and work-zone context) with the data-availability mask.

F. Model Architecture and Adaptive Conformal Prediction (ACP)

We leverage a Spatio-Temporal Transformer model [47] with an encoder-decoder design (STT-ED) to perform multi-horizon traffic forecasting, exploiting the inherent parallel sequence architecture of a transformer. Let the traffic flow tensor be $\mathbf{F} \in \mathbb{R}^{T \times N}$, where $N = |\mathcal{V}|$ sensors and T is the number of time samples. For each training sample, we form an input window of length L and predict the next H steps:

$$\mathbf{X}_t = \mathbf{F}_{t-L+1:t} \in \mathbb{R}^{L \times N}, \quad \mathbf{Y}_t = \mathbf{F}_{t+1:t+H} \in \mathbb{R}^{H \times N} \quad (28)$$

As our spatial information is hour-conditioned, each window is characterized by an hour-of-day index $h_t \in \{0, \dots, 23\}$, extracted from the timestamp of the last step in the window. Now $\mathbf{A}_{\text{adaptive}}^{(h)}$ is injected in the spatial module of the model by selecting the appropriate matrix based on the window hour h_t . Then, a row-normalized version is implemented for graph mixing:

$$\tilde{\mathbf{A}}_t = \text{RowNorm}\left(\mathbf{A}_{\text{adaptive}}^{(h_t)} + \mathbf{I}\right) \quad (29)$$

$$\text{RowNorm}(\mathbf{M})[i, j] = \frac{\mathbf{M}[i, j]}{\sum_k \mathbf{M}[i, k] + \varepsilon} \quad (30)$$

Temporal Tokenization and Temporal Encoder: Unlike recurrent models, the Transformer processes a sequence of tokens. For each node i , it treats L -step history as a 1D sequence and converts it into patch tokens using a temporal convolution with patch length p [80] (e.g., $p = 6$ for 90-min patches with 15-min data). Let $x_{t,i} \in \mathbb{R}^L$ denote the input history for node i . The tokens are formed as:

$$\mathbf{Z}_{t,i}^{(0)} = \text{PatchConv}(x_{t,i}) \in \mathbb{R}^{L_p \times d}, \quad L_p = \left\lfloor \frac{L}{p} \right\rfloor \quad (31)$$

where d is the Transformer embedding dimension. We add sinusoidal positional encoding $\text{PE}(\cdot)$ to preserve temporal ordering as:

$$\mathbf{Z}_{t,i}^{(0)} \leftarrow \mathbf{Z}_{t,i}^{(0)} + \text{PE} \quad (32)$$

The temporal encoder comprises D_t stacked Transformer encoder blocks. For a generic encoder layer ℓ , multi-head self-attention (MHSA) is computed as:

$$\mathbf{Q} = \mathbf{Z}^{(\ell-1)} \mathbf{W}_Q \quad (33)$$

$$\mathbf{K} = \mathbf{Z}^{(\ell-1)} \mathbf{W}_K \quad (34)$$

$$\mathbf{V} = \mathbf{Z}^{(\ell-1)} \mathbf{W}_V \quad (35)$$

$$\text{Attn}(\mathbf{Q}, \mathbf{K}, \mathbf{V}) = \text{softmax}\left(\frac{\mathbf{Q}\mathbf{K}^\top}{\sqrt{d_k}}\right) \mathbf{V} \quad (36)$$

With residual connections and layer normalization (LN), the temporal encoder update is:

$$\hat{\mathbf{Z}}^{(\ell)} = \text{LN}\left(\mathbf{Z}^{(\ell-1)} + \text{Dropout}(\text{MHSA}(\mathbf{Z}^{(\ell-1)}))\right) \quad (37)$$

$$\mathbf{Z}^{(\ell)} = \text{LN}\left(\hat{\mathbf{Z}}^{(\ell)} + \text{FFN}(\hat{\mathbf{Z}}^{(\ell)})\right) \quad (38)$$

where $\text{FFN}(\cdot)$ is a two-layer MLP with nonlinearity. The output of the temporal encoder produces per-node temporal memories $\mathbf{M}_{t,i}^{\text{time}} \in \mathbb{R}^{L_p \times d}$.

Adjacency Matrix Integration with Spatial Module: To integrate the hour-conditioned adjacency matrix in the spatial module, temporal tokens are pooled using global average pooling as:

$$\mathbf{u}_{t,i} = \text{Pool}(\mathbf{M}_{t,i}^{\text{time}}) \in \mathbb{R}^d \quad (39)$$

We then learn a trainable node embedding $\mathbf{e}_i \in \mathbb{R}^d$ to encode each station identity as:

$$\mathbf{h}_{t,i}^{(0)} = \mathbf{u}_{t,i} + \mathbf{e}_i \quad (40)$$

Now, stacking all the nodes results in $\mathbf{H}_t^{(0)} \in \mathbb{R}^{N \times d}$. Then, we inject the hour-conditioned adaptive adjacency using:

$$\mathbf{H}_t^{\text{mix}} = \tilde{\mathbf{A}}_t \mathbf{H}_t^{(0)} \in \mathbb{R}^{N \times d} \quad (41)$$

This is the key mechanism by which $\mathbf{A}^{(h)}$ directly used in the neural representation. Before the spatial attention is applied, the node embeddings are already skewed by the incident/variability-aware connectivity for the corresponding hour-of-day.

Spatial Transformer Encoder: After the integration of hour-conditioned adjacency matrix, we refine the spatial interactions using a spatial Transformer encoder consisting of D_s stacked encoder blocks operating over the nodes. We start the spatial encoder from the graph-mixed representation. That is, the output of the adjacency-based mixing step becomes the spatial encoder's initial hidden state, $\mathbf{H}_t^{(0,s)} = \mathbf{H}_t^{\text{mix}}$. This just ensures, the hour-conditioned spatial graphs are included in the spatial tokens before attention is learned. After the spatial encoder, each node embedding is treated as a single spatial token:

$$\mathbf{s}_{t,i} = \mathbf{H}_t^{(D_s,s)}[i, :] \in \mathbb{R}^d, \quad i = 1, \dots, N \quad (42)$$

Long-Horizon Decoding with Cross-Attention: After the temporal encoder and the spatial encoder, each node i has temporal memory tokens $\mathbf{M}_{t,i}^{\text{time}}$, and a spatial token $\mathbf{s}_{t,i}$. Now, a decoder memory is created by concatenation:

$$\mathbf{M}_{t,i} = \left[\mathbf{M}_{t,i}^{\text{time}} \parallel \mathbf{s}_{t,i} \right] \in \mathbb{R}^{(L_p+1) \times d} \quad (43)$$

TABLE II
SAMPLE ODOT CRASH DATASET

Crash Date/time	Weather	Latitude	Longitude	Functional Class	Vehicle (mph)	Speed (mph)	Speed Limit	Work Zone	ICT (min)
11/19/2023 11:43	1	40.111327	-83.002978	1	50	65	N		67
05/16/2023 06:50	2	39.832623	-82.736814	3	40	60	N		115
06/19/2023 12:13	2	39.945520	-81.985450	1	50	50	Y		64
...									
11/22/2023 15:25	2	39.931881	-82.907888	1	75	70	N		50
Weather code: 1=Clear, 2=Cloudy, 3=Fog/Smog/Smoke, 4=Rain, 5=Sleet/Hail, 6=Snow, 7=Severe Crosswinds, 8=Blowing Sand/Soil/Dirt/Snow, 9=Freezing Rain/Drizzle, 99=Other/Unknown									
Functional class code: 1-2=Interstates/Freeways, 3=Principal Arterial, 4=Minor Arterial, 5-6=Collector Roads, 7=Local Roads									
Work zone: Y=Yes, N=No									

To forecast the next H steps, we use an H -length learnable query seed $\mathbf{Q}_0 \in \mathbb{R}^{H \times d}$ (tiled per node) and decode using a standard Transformer decoder. At each decoder layer, the query first looks at itself (to couple horizons) and then cross-attends to the memory block:

$$\mathbf{Q}'_{t,i} = \text{Attn}(\mathbf{Q}_{t,i}, \mathbf{Q}_{t,i}, \mathbf{Q}_{t,i}) \quad (44)$$

$$\mathbf{Q}_{t,i} \leftarrow \text{Attn}(\mathbf{Q}'_{t,i}, \mathbf{M}_{t,i}, \mathbf{M}_{t,i}) \quad (45)$$

Finally, the decoded representation is mapped to the H -step flow forecast for node i by a linear head:

$$\hat{\mathbf{Y}}_t[:, i] = \mathbf{Q}_{t,i} \mathbf{W}_o + \mathbf{b}_o, \quad \hat{\mathbf{Y}}_t \in \mathbb{R}^{H \times N} \quad (46)$$

Adaptive Conformal Prediction (ACP) for Multi-Horizon Intervals: Following our prior work [8], we estimate uncertainty via ACP with epoch-wise adaptive calibration. After each training epoch (and once after early-stopping selects the final checkpoint), we compute calibration residuals on the held-out validation set:

$$r_{t,k,i} = \left| \hat{\mathbf{Y}}_{t,k,i} - Y_{t,k,i} \right|, \quad (47)$$

and obtain horizon- and node-specific conformal radii as

$$q_{k,i}^{(1-\alpha)} = \text{Quantile}_{1-\alpha} \left(\{r_{t,k,i}\}_{t \in \mathcal{D}_{\text{cal}}} \right). \quad (48)$$

The resulting prediction intervals are

$$\hat{\mathbf{Y}}_{t,k,i} - q_{k,i}^{(1-\alpha)} \leq Y_{t,k,i} \leq \hat{\mathbf{Y}}_{t,k,i} + q_{k,i}^{(1-\alpha)}. \quad (49)$$

Here $q_{k,i}^{(1-\alpha)}$ is computed per horizon and per node to reflect increasing uncertainty with k and spatial heterogeneity.

Overall architecture of the proposed Spatio-Temporal Transformer with Adaptive Conformal Prediction (STT-ED-ACP) is shown in Figure 2. The STT takes as input a traffic flow window \mathbf{X}_t and the corresponding hour-of-day tag h_t , and produces multi-horizon point forecasts $\hat{\mathbf{Y}}_t$. Crash attributes and baseline travel times are used to construct an hour-conditioned, incident-aware adjacency matrices $\{\mathbf{A}^{(h)}\}_{h=0}^{23}$, from which the appropriate adjacency is selected based on h_t and injected via graph-weighted mixing in the spatial encoder. ACP is applied as a post-forecast calibration layer to generate horizon- and node-specific prediction intervals.

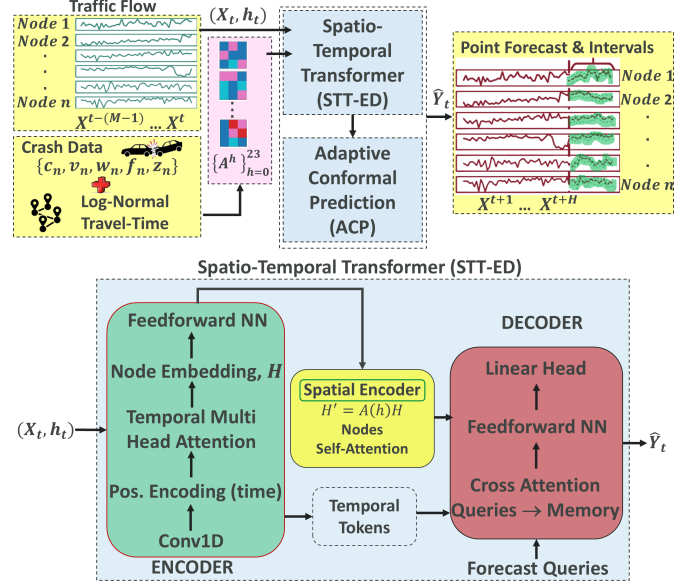


Fig. 2. Spatio-Temporal Transformer (STT-ED) architecture with hour-conditioned adaptive adjacency and Adaptive Conformal Prediction (ACP) for multi-horizon traffic forecasting

IV. RESULTS AND DISCUSSION

We evaluate the proposed STT-ED framework on 2023 ODOT traffic data and the corresponding ODOT crash records (also reported to the Ohio Department of Public Safety (ODPS)). We set prediction horizons of 1 hr, 2 hr, 3 hr, and 4 hr, with a 24-hour historical look-back period. All models, including the ablation variants, were trained with early stopping (patience = 10) and a maximum of 20 epochs. All experiments are conducted on the full network with $N = 273$ nodes, yielding a 273×273 travel-time-based adjacency (N^2 node pairs). We found 20,046 total crashes in Ohio for 2023. Table II shows a sample of the crash dataset used to build the incident-aware attribute signals.

A. Baseline Methods and Evaluation Metrics

We selected the following baseline models for comparative analysis using the same inputs and incident-aware adjacency as the proposed model:

- 1) Historical Average (HA) [81]: Predicts traffic flow using the historical mean computed from the training data.

- 2) Autoregressive Integrated Moving Average (ARIMA) [82]: Classical univariate statistical forecasting model, capturing autoregressive and moving-average dynamics.
- 3) Feedforward Neural Network (FNN): Multilayer perceptron capturing non-linear relationships.
- 4) GCN-GRU [19]: Using gated recurrent units (GRU) for temporal modeling to reduce parameter count and improve computational efficiency.
- 5) GAT-LSTM [8]: Using graph attention (GAT) to learn adaptive spatial weights, followed by LSTM-based temporal forecasting.
- 6) STGCN [23]: Spatio-temporal graph convolutional network that jointly models spatial and temporal dependencies using graph convolutions and gated temporal convolutions.
- 7) DCRNN [24]: Diffusion convolutional recurrent neural network that integrates diffusion-based graph convolutions with a sequence-to-sequence recurrent architecture for multi-step forecasting.
- 8) Graph WaveNet [28]: Dilated temporal convolutional network augmented with adaptive graph learning and diffusion graph convolutions for long-range spatio-temporal dependencies.
- 9) ASTGCN [26]: Attention-based spatio-temporal graph convolutional network that models both spatial and temporal attention mechanisms within a Chebyshev graph convolution framework.

We report standard accuracy metrics for multi-horizon prediction, aggregated over all nodes and forecast steps. Mean Absolute Error (MAE) is:

$$\text{MAE} = \frac{1}{|\Omega|} \sum_{(t,k,i) \in \Omega} |Y_{t,k,i} - \hat{Y}_{t,k,i}|, \quad (50)$$

and Root Mean Squared Error (RMSE) is:

$$\text{RMSE} = \sqrt{\frac{1}{|\Omega|} \sum_{(t,k,i) \in \Omega} (Y_{t,k,i} - \hat{Y}_{t,k,i})^2}, \quad (51)$$

where Ω denotes the evaluation set over time indices t , horizons $k \in \{1, \dots, H\}$, and nodes $i \in \{1, \dots, N\}$.

To evaluate calibrated uncertainty, we report Prediction Interval Coverage Probability (PICP) and Mean Prediction Interval Width (MPIW) using ACP intervals:

$$\text{PICP} = \frac{1}{|\Omega|} \sum_{(t,k,i) \in \Omega} \mathbf{1}(\hat{Y}_{t,k,i}^L \leq Y_{t,k,i} \leq \hat{Y}_{t,k,i}^U), \quad (52)$$

$$\text{MPIW} = \frac{1}{|\Omega|} \sum_{(t,k,i) \in \Omega} (\hat{Y}_{t,k,i}^U - \hat{Y}_{t,k,i}^L), \quad (53)$$

where $[\hat{Y}_{t,k,i}^L, \hat{Y}_{t,k,i}^U]$ is the conformal prediction interval at horizon k and node i . As in our prior work, we omit MAPE because near-zero flows can inflate or render percentage errors undefined, while MAE/RMSE remain stable.

B. Adjacency Analysis and Performance Comparison

To ensure a controlled and interpretable comparison across all models, we evaluate performance on a fixed subset of

$N = 50$ representative stations, corresponding to a connected route segment within the study network. Figure 3 illustrates the selected route, traffic count stations, and crash sites. We select this particular Columbus route segment as the length of the route is approximately 47.5 miles (typically varying from 1 hour to 1 hour 30 minutes), which enables repeatable long-run experiments without requiring a much larger corridor-scale network. While a natural alternative would be to validate long-horizon forecasting on a single 4+ hour interstate corridor traversal, doing so would require continuous multi-state data coverage and consistent incident/ground-truth alignment across jurisdictions. Since our study is based on Ohio-only datasets (ODOT traffic counts and ODOT crash records), we adopt a loop-based experimental design on a Columbus corridor to emulate extended trips while remaining fully supported by the available data sources. Also, since our objective is long-horizon forecasting, we require extended scenarios to evaluate how prediction quality evolves as conditions transition across the day. Therefore, we are imitating a travel that executes “four” repeated loop runs over the same segment, which effectively spans off-peak to peak (or peak to off-peak) regimes within a single experiment. This design provides a consistent and efficient way to generate long-duration test scenarios while preserving identical spatial structure, and it enables a controlled validation task while undertaking SUMO Monte Carlo simulations.

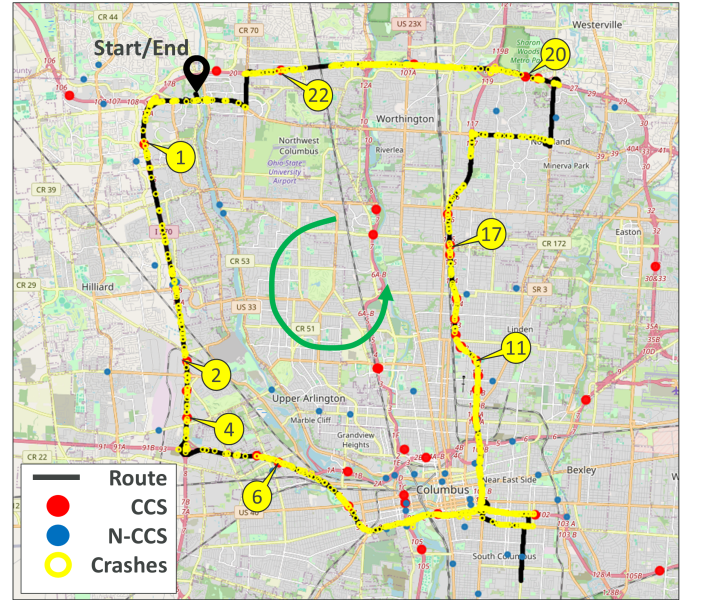


Fig. 3. Sampled Traffic Route

Beyond predictive accuracy, we analyze how incorporating crash context alters the underlying spatial connectivity used by the forecasting models. Figure 4 visualizes the change in adjacency weights:

$$\Delta \mathbf{A}^{(h)} = \mathbf{A}_{\text{crash}}^{(h)} - \mathbf{A}_{\text{base}}^{(h)}$$

for four afternoon hours ($h = 14 : 00 - 17 : 00$), where $\mathbf{A}_{\text{base}}^{(h)}$ is constructed using $\text{CV}(h)$ travel-time sampling, and $\mathbf{A}_{\text{crash}}^{(h)}$ further incorporates crash severity. The predominantly negative

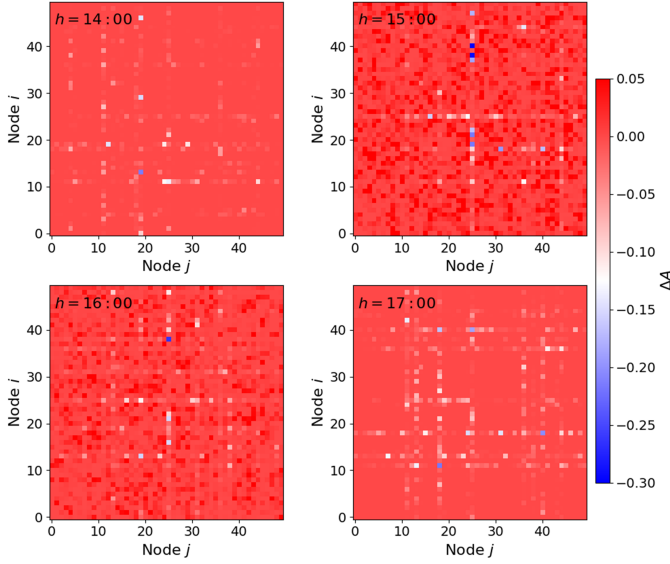


Fig. 4. Crash-induced change in adjacency weights across selected hours

$\Delta A^{(h)}$ values indicate that crash-induced increases in effective travel time reduce graph connectivity through the travel-time kernel, thereby weakening spatial coupling between affected nodes. Importantly, the magnitude and spatial pattern of these changes vary by hour, highlighting the time-dependent impact of incidents on the network.

Table III presents the MAE and RMSE for each method across multi-hour prediction windows.

TABLE III
PREDICTION PERFORMANCE COMPARISON

Method	MAE				RMSE			
	1h	2h	3h	4h	1h	2h	3h	4h
HA	0.921/0.921/0.921/0.921				0.991/0.991/0.991/0.991			
ARIMA	0.136/0.327/0.520/0.674				0.191/0.413/0.608/0.752			
FNN	0.357/0.380/0.389/0.392				0.511/0.558/0.569/0.571			
GCN-GRU	0.310/0.326/0.347/0.401				0.394/0.426/0.490/0.511			
GAT-LSTM	0.251/0.265/0.362/0.426				0.363/0.370/0.477/0.514			
STGCN	0.321/0.323/0.335/0.359				0.418/0.419/0.462/0.472			
DCRNN	0.098/0.227/0.360/0.486				0.148/0.321/0.474/0.614			
Graph WaveNet	0.122/0.233/0.350/0.485				0.157/0.282/0.422/0.601			
ASTGCN	0.128/0.228/0.329/0.332				0.162/0.311/0.432/0.461			
STT-ED	0.087/0.214/0.291/0.317				0.138/0.277/0.374/0.413			

It can be observed that the strongest competitors to STT-ED are the graph-based baselines (notably DCRNN, Graph WaveNet, ASTGCN, and GAT-LSTM), which consistently outperform classical approaches by leveraging spatial correlations across stations. However, most of these methods exhibit larger error growth as the horizon increases, indicating sensitivity to long-horizon uncertainty propagation and limited temporal modeling capacity under distribution shifts. In contrast, STT-ED achieves the best MAE/RMSE across all horizons and shows the most stable scaling with horizon length, suggesting that the encoder-decoder Transformer structure (with cross-attention decoding) is more effective for long-horizon forecasting.

C. Prediction Results

Figure 5 illustrates multi-horizon traffic flow predictions and corresponding ACP uncertainty intervals for Node 1 (see Figure 3). As the forecast horizon increases from 1 to 4 hours, the prediction uncertainty widens, reflecting the accumulation of temporal uncertainty, while the point forecasts continue to capture the dominant patterns and peak-off-peak transitions. Notably, the ACP intervals expand around periods of higher variability, indicating effective uncertainty calibration without overly conservative bounds.

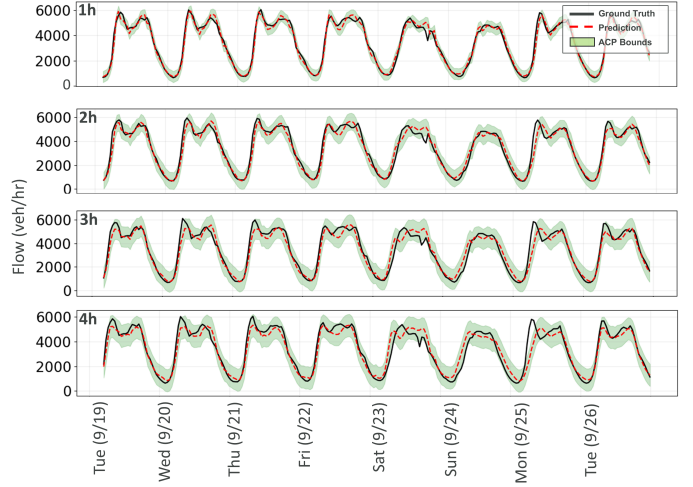


Fig. 5. Traffic Prediction with Uncertainty Bounds (Node 1)

D. Uncertainty Quantification

To evaluate the effectiveness of the proposed Adaptive Conformal Prediction (ACP) framework, we benchmark it against the following baselines:

- 1) Gaussian Process Regression (GPR) [83]: Probabilistic regression framework that yields predictive distributions by utilizing kernel-based Bayesian formulation.
- 2) Mean-Variance Estimation (MVE) [84]: Jointly predicts the conditional mean and variance, enabling uncertainty-aware point forecasts.
- 3) Deep Ensembles (DE) [75]: Quantifying uncertainty by aggregating predictions from multiple independently trained neural networks.
- 4) Quantile Regression (QR) [85]: Estimates conditional quantiles, allowing prediction intervals to be constructed without distributional assumptions.
- 5) Bootstrap Aggregation (BA) [86]: Estimates predictive variability by training multiple models on resampled training data.
- 6) Conformal Prediction (CP) [76]: A distribution-free uncertainty quantification method constructing prediction intervals using residuals from calibration set.
- 7) Conformalized Quantile Regression (CQR) [77]: Combines quantile regression with conformal calibration to produce adaptive prediction intervals.

These methods serve as strong baselines for assessing calibration quality and interval efficiency of the proposed

ACP approach under multi-horizon traffic forecasting settings. Table IV reports PICP and MPIW metrics.

TABLE IV
UNCERTAINTY QUANTIFICATION BOUNDS COMPARISON

Method	PICP %	MPIW
	1h / 2h / 3h / 4h	1h / 2h / 3h / 4h
GPR	66.64/89.65/88.20/90.11	0.372/3.298/3.303/3.296
MVE	89.34/90.51/91.02/91.44	0.952/1.221/2.565/2.747
DE	71.03/73.10/75.65/77.81	0.701/0.882/1.034/1.175
QR	67.76/66.32/65.57/66.06	0.504/0.655/0.768/0.832
BA	43.74/37.22/36.74/35.50	0.226/0.246/0.251/0.258
CP	90.10/91.50/89.38/89.44	0.571/1.910/2.231/2.895
CQR	91.95/91.47/90.87/90.76	0.668/1.971/1.896/1.458
ACP	94.09/93.51/91.13/92.94	0.582/0.876/1.036/1.148

ACP provides the best coverage among the strongest competitors (CP and CQR). Compared to CP, ACP maintains similar (and often slightly higher) PICP while producing substantially tighter intervals, with MPIW reductions of roughly ~ 53 - 60% for the 2h-4h horizons. Relative to CQR, ACP achieves comparable coverage but notably narrower bounds at 2h-3h (about ~ 45 - 55% smaller MPIW), while remaining competitive at 4h. Overall, ACP delivers higher coverage while maintaining the tightest (or near-tightest) uncertainty bands among the conformal baselines.

E. Ablation Study

To isolate the contribution of each architectural block in the proposed STT framework, we perform an ablation study by removing components from the full encoder-decoder model. In particular, we compare five configurations:

- 1) STT-ED (Full): the complete encoder-decoder Transformer used in our main experiments.
- 2) STT-E (Encoder-only): removes the decoder cross-attention and directly maps learned spatio-temporal embeddings to multi-horizon forecasts.
- 3) STT-D (Decoder-only): removes the encoder stack and relies on learned horizon queries with a lightweight memory representation to generate multi-step predictions.
- 4) STT-ED-NoPatch: removes the temporal patch tokenization (Conv1D tokenization) and instead uses step-wise tokenization, testing the effect of patch-based temporal embedding.
- 5) STT-ED-NoCrossAttn: removes the decoder cross-attention to the encoder memory, testing whether explicit encoder-decoder information flow is necessary for long-horizon decoding.

Table V reports MAE/RMSE across the multi-hour horizons. The ablation findings confirm that the full STT-ED achieves the best accuracy and degrades gracefully with horizon, indicating that both the encoder memory and decoder cross-attention are key for stable long-horizon decoding. Removing patch tokenization (STT-ED-NoPatch) produces a consistent error increase across horizons from 1h to 4h, suggesting that temporal patching mainly improves representation efficiency

TABLE V
ABLATION STUDY UNDER DIFFERENT STT CONFIGURATIONS

Configuration	MAE	RMSE
	1h / 2h / 3h / 4h	1h / 2h / 3h / 4h
STT-ED	0.087/0.214/0.291/0.317	0.138/0.277/0.374/0.413
STT-ED-NoPatch	0.101/0.238/0.304/0.323	0.142/0.297/0.382/0.461
STT-ED-NoCrossAttn	0.736/0.720/0.719/0.722	0.773/0.789/0.786/0.791
STT-E	0.096/0.221/0.303/0.327	0.151/0.289/0.386/0.425
STT-D	0.137/0.249/0.297/0.322	0.178/0.351/0.383/0.421

and robustness at longer horizons. The encoder-only variant (STT-E) remains close to the full model (MAE within $+0.009$ to $+0.012$; RMSE within $+0.013$ to $+0.019$), while the decoder-only variant (STT-D) is notably worse at 1h-2h (MAE $+0.050/+0.035$; RMSE $+0.040/+0.074$) but becomes competitive by 4h, implying that the encoder’s temporal token memory is particularly beneficial for near-term dynamics. In contrast, removing decoder cross-attention (STT-ED-NoCrossAttn) causes a severe collapse (MAE ≈ 0.72 - 0.74 ; RMSE ≈ 0.77 - 0.79), demonstrating that explicit encoder-to-decoder information flow is essential for producing meaningful multi-horizon forecasts in this architecture.

F. Model Validation with Multi-Hour Simulation

To validate the proposed forecasting framework under realistic, time-varying conditions, we extend the simulation-based evaluation strategy used in our prior work [87] to a multi-hour setting. Unlike single-hour validation, this experiment explicitly assesses the model’s ability to propagate traffic dynamics as network demand evolves across consecutive hours.

Using the same sampled route described in Section IV-B, we conduct microscopic traffic simulations in SUMO driven by the model’s predicted traffic flows for the selected time periods. For each experiment, the STT produces hourly forecasts for all stations along the route, and these predicted flows are injected into SUMO to construct a four-hour traffic scenario. As a result, network demand is updated at each simulated hour, enabling evaluation under realistic transitions between off-peak and peak conditions. The route characteristics are outlined in Table VI.

TABLE VI
ROUTE CHARACTERISTICS

Parameter	Value
Route Length (mi)	47.5
Number of Intersections	84
Number of Traffic Lights	39
Number of Lanes (per direction)	1-5
Functional Class	Interstates/freeways, arterials, collectors and locals
Mean Speed (mph)	74.5 (TOD range: 63.2-80.0)
INRIX congestion indicator (%)	95.9 (Historic average: 96.3)

We focus on two representative peak regimes as shown in Figure 6 as observed in historical INRIX travel-time data. There is a daytime peak from 10:00 AM to 2:00 PM and an evening peak from 6:00 PM to 10:00 PM. The INRIX data represents single-trip travel times for the selected 47.5-mile

route, aggregated by departure hour (i.e., one traversal of the corridor). For each scenario, we simulate a 200-run Monte Carlo simulation to cover the variability pattern.

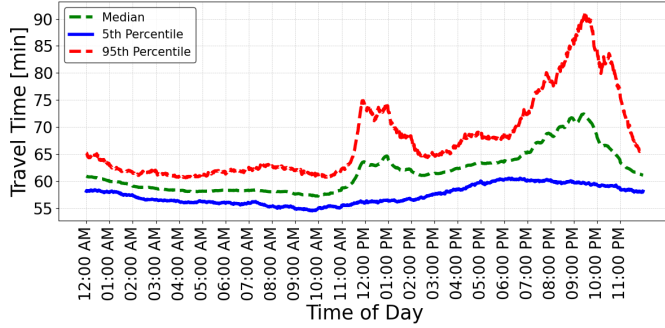


Fig. 6. INRIX historical travel time data

Figure 7 shows INRIX corridor heatmaps for two representative departure times (12:00 and 21:00), illustrating the spatial heterogeneity of congestion along the route. We use these plots as qualitative context to identify recurrent hotspots and support the selection of peak regimes, rather than as direct simulation ground truth.

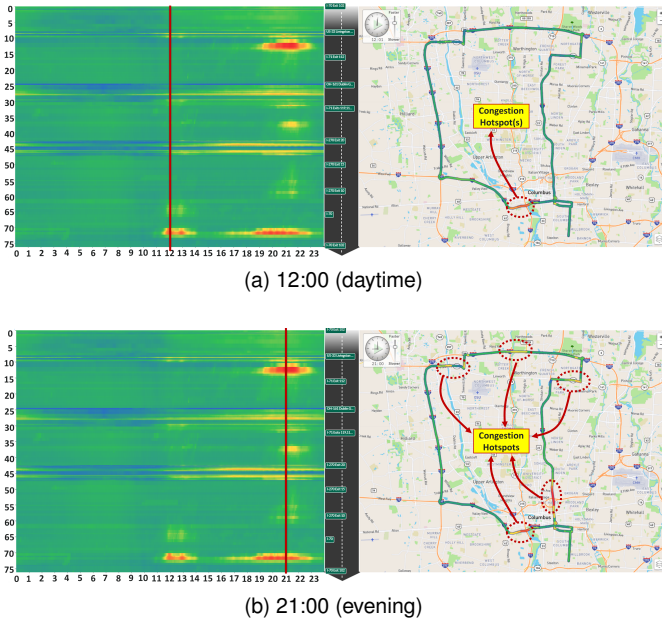


Fig. 7. INRIX Congestion Heatmaps

At each Monte Carlo run, a Vehicle Under Test (VUT) navigates the route “four” times; each run consists of multiple sequential traversals, during which traffic flow values are updated hourly based on the model’s forecasts. Figure 8 compares the resulting simulated travel-time distributions for the two peak regimes, which explains the shift in the distribution support (approximately 220-330 minutes) relative to the INRIX single-trip statistics (approximately 55-85 minutes). The observed widening of the evening-peak distribution is consistent with the compounding effects of congestion and stop-and-go dynamics across successive peak hours.

Kolmogorov–Smirnov (KS) tests further confirm that the simulated travel-time samples follow a log-normal distribution

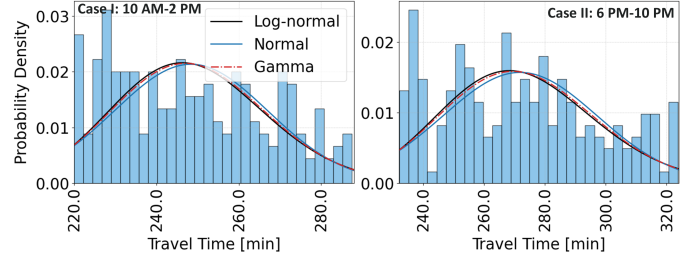


Fig. 8. SUMO Travel time distribution (Simulated)

in both cases, validating the distributional assumption used in the hour-conditioned adjacency formulation.

- Case I (Daytime Peak): log-normal (KS = 0.078/ p = 0.156), normal (KS = 0.088/ p = 0.081), gamma (KS = 0.0809/ p = 0.137)
- Case II (Evening Peak): log-normal (KS = 0.066/ p = 0.333), normal (KS = 0.083/ p = 0.116), gamma (KS = 0.071/ p = 0.245)

Lower KS and $p > 0.05$ for log-normal validate both the assumed distribution and simulation fidelity.

V. CONCLUSION

In this work, we proposed an STT-ED forecasting framework with Adaptive Conformal Prediction (STT-ED-ACP) for long-horizon traffic prediction under time-varying and incident-driven conditions. The key idea is to replace static spatial connections with an hour-conditioned, incident-aware adjacency matrix by parameterizing travel-time variability using a piecewise $CV(h)$ profile (log-normal sampling) and perturbing edge weights using crash-derived severity signals. The encoder-decoder Transformer leverages parallel temporal attention and cross-attention decoding, while the selected $A^{(h_i)}$ is injected into the spatial encoder to reflect prevailing network conditions within each forecasting window. Across all multi-hour horizons, STT-ED achieves the best MAE/RMSE with slower error growth, and ACP provides near-nominal coverage with tight, horizon-dependent prediction intervals, especially during regime transitions. Finally, multi-hour SUMO loop validation shows realistic travel-time distributions consistent with INRIX observations, supporting both the log-normal travel-time assumption and the model’s ability to propagate network dynamics over extended horizons.

Despite these encouraging results, several limitations remain. First, the hour-conditioned CV profile is estimated from historical data and treated as fixed during inference; while this captures systematic diurnal patterns, it does not adapt online to unexpected demand surges or large-scale events. Second, crash information is incorporated through aggregated severity signals rather than through explicit spatio-temporal incident evolution, which may oversimplify complex queue formation and dissipation processes. Third, the current study focuses on a single regional network and a fixed set of horizons; broader generalization across cities, seasons, and sensing resolutions remains to be explored. Finally, ACP calibration is performed epoch-wise rather than fully online, which may limit responsiveness under abrupt distribution shifts.

Future work will focus on extending to scaling the approach to larger networks and longer horizons, as well as integrating the framework into real-time decision-support pipelines for traffic management and traveler information systems, also remain important avenues for continued research.

REFERENCES

- [1] B. Pishue, "2024 INRIX Global Traffic Scorecard," INRIX Research, June 2025.
- [2] National Highway Traffic Safety Administration (NHTSA), National Center for Statistics and Analysis, "Summary of Motor Vehicle Traffic Crashes: 2023 Data," Crash Stats, DOT HS 813 762, Oct. 2025. [Online]. Available: <https://crashstats.nhtsa.dot.gov/Api/Public/ViewPublication/813762>
- [3] National Highway Traffic Safety Administration (NHTSA), National Center for Statistics and Analysis, "Early Estimate of Motor Vehicle Traffic Fatalities in 2024," Crash Stats, DOT HS 813 710, Apr. 2025. [Online]. Available: <https://crashstats.nhtsa.dot.gov/Api/Public/ViewPublication/813710>
- [4] Federal Highway Administration (FHWA), "Road Weather Management Overview," Office of Operations, U.S. Department of Transportation. [Online]. Available: <https://ops.fhwa.dot.gov/weather/overview.htm>
- [5] M. Xu, W. Dai, C. Liu, X. Gao, W. Lin, G.-J. Qi, and H. Xiong, "Spatial-Temporal Transformer Networks for Traffic Flow Forecasting," *IEEE Trans. Intelligent Transportation Systems* (preprint), 2020.
- [6] L. Cai, K. Janowicz, G. Mai, B. Yan, and R. Zhu, "Traffic Transformer: Capturing the Continuity and Periodicity of Time Series for Traffic Forecasting," *Transactions in GIS*, 2020.
- [7] H. Yan, X. Ma, and Z. Pu, "Learning Dynamic and Hierarchical Traffic Spatiotemporal Features With Transformer," *IEEE Trans. Intelligent Transportation Systems*, vol. 23, no. 11, pp. 22386-22399, 2022.
- [8] M. Patil, Q. Ahmed, and S. Midlam-Mohler, "Travel Time and Weather-Aware Traffic Forecasting in a Conformal Graph Neural Network Framework," *IEEE Transactions on Intelligent Transportation Systems*, early access, 2025, doi: 10.1109/TITS.2025.3611267.
- [9] Y. Shen, J. Xu, X. Wu, and Y. Ni, "Modelling travel time distribution and its influence over stochastic vehicle scheduling," *Transport*, vol. 34, no. 2, pp. 237-249, 2019.
- [10] E. Mazloumi, G. Currie, and G. Rose, "Using GPS data to gain insight into public transport travel time variability," *J. Transp. Eng.*, vol. 136, no. 7, pp. 623-631, 2010.
- [11] G. E. P. Box, G. M. Jenkins, G. C. Reinsel, and G. M. Ljung, *Time Series Analysis: Forecasting and Control*, 5th ed. Hoboken, NJ, USA: Wiley, 2015.
- [12] R. G. Brown, *Smoothing, Forecasting and Prediction of Discrete Time Series*. Englewood Cliffs, NJ, USA: Prentice-Hall, 1963.
- [13] C. C. Holt, "Forecasting trends and seasonals by exponentially weighted moving averages," in *Proc. Int. Symp. Forecasting*, Carnegie Inst. Technol., Pittsburgh, PA, USA, 1957, republished in *Int. J. Forecasting*, vol. 20, no. 1, pp. 5-10, 2004.
- [14] P. R. Winters, "Forecasting sales by exponentially weighted moving averages," *Manage. Sci.*, vol. 6, no. 3, pp. 324-342, 1960.
- [15] R. J. Hyndman, A. B. Koehler, R. D. Snyder, and S. Grose, "A state space framework for automatic forecasting using exponential smoothing," *Int. J. Forecasting*, vol. 18, no. 3, pp. 439-454, 2002.
- [16] M. Lippi, M. Bertini, and P. Frasconi, "Short-term traffic flow forecasting: An experimental comparison of time-series analysis and supervised learning," *IEEE Trans. Intell. Transp. Syst.*, vol. 14, no. 2, pp. 871-882, 2013.
- [17] Y. Lv, Y. Duan, W. Kang, Z. Li, and F.-Y. Wang, "Traffic Flow Prediction With Big Data: A Deep Learning Approach," *IEEE Transactions on Intelligent Transportation Systems*, vol. 16, no. 2, pp. 865-873, Apr. 2015, doi: 10.1109/TITS.2014.2345663.
- [18] X. Ma, Z. Tao, Y. Wang, H. Yu, and Y. Wang, "Long short-term memory neural network for traffic speed prediction using remote microwave sensor data," *Transp. Res. C Emerg. Technol.*, vol. 54, pp. 187-197, May 2015.
- [19] R. Fu, Z. Zhang, and L. Li, "Using LSTM and GRU neural network methods for traffic flow prediction," in *Proc. 2016 31st Youth Academic Annu. Conf. Chinese Assoc. Autom. (YAC)*, Wuhan, China, 2016, pp. 324-328, doi: 10.1109/YAC.2016.7804912.
- [20] G. Lai, W.-C. Chang, Y. Yang, and H. Liu, "Modeling Long- and Short-Term Temporal Patterns with Deep Neural Networks," in *Proc. 41st Int. ACM SIGIR Conf. Research and Development in Information Retrieval (SIGIR)*, Ann Arbor, MI, USA, 2018, pp. 95-104, doi: 10.1145/3209978.3210006.
- [21] S. Bai, J. Z. Kolter, and V. Koltun, "An Empirical Evaluation of Generic Convolutional and Recurrent Networks for Sequence Modeling," *arXiv preprint arXiv:1803.01271*, 2018.
- [22] Y. Qin, D. Song, H. Chen, W. Cheng, G. Jiang, and G. Cottrell, "A Dual-Stage Attention-Based Recurrent Neural Network for Time Series Prediction," in *Proc. 26th Int. Joint Conf. Artificial Intelligence (IJCAI)*, 2017, pp. 2627-2633.
- [23] B. Yu, H. Yin, and Z. Zhu, "Spatio-temporal graph convolutional networks: A deep learning framework for traffic forecasting," *arXiv preprint arXiv:1709.04875*, 2017.
- [24] Y. Li, R. Yu, C. Shahabi, and Y. Liu, "Diffusion convolutional recurrent neural network: Data-driven traffic forecasting," *arXiv preprint arXiv:1707.01926*, 2017.
- [25] L. Zhao, Y. Song, C. Zhang, Y. Liu, P. Wang, T. Lin, et al., "T-GCN: A temporal graph convolutional network for traffic prediction," *IEEE Transactions on Intelligent Transportation Systems*, vol. 21, no. 9, pp. 3848-3858, 2019.
- [26] S. Guo, Y. Lin, N. Feng, C. Song, and H. Wan, "Attention based spatial-temporal graph convolutional networks for traffic flow forecasting," in *Proceedings of the AAAI Conference on Artificial Intelligence*, vol. 33, no. 01, pp. 922-929, July 2019.
- [27] Z. Cui, K. Henrickson, R. Ke, and Y. Wang, "Traffic Graph Convolutional Recurrent Neural Network: A Deep Learning Framework for Network-Scale Traffic Learning and Forecasting," *IEEE Transactions on Intelligent Transportation Systems*, vol. 21, no. 11, pp. 4883-4894, Nov. 2020, doi: 10.1109/TITS.2019.2950416.
- [28] Z. Wu, S. Pan, G. Long, J. Jiang, and C. Zhang, "Graph WaveNet for deep spatial-temporal graph modeling," *arXiv preprint arXiv:1906.00121*, 2019.
- [29] C. Zheng, X. Fan, C. Wang, and J. Qi, "GMAN: A graph multi-attention network for traffic prediction," in *Proceedings of the AAAI Conference on Artificial Intelligence*, vol. 34, no. 01, pp. 1234-1241, April 2020.
- [30] G. Li, V. L. Knoop, and J. W. C. van Lint, "Multistep traffic forecasting by dynamic graph convolution: Interpretations of real-time experiments," *Transportation Research Part C: Emerging Technologies*, vol. 128, art. no. 103185, 2021, doi: 10.1016/j.trc.2021.103185.
- [31] Y. Shin and Y. Yoon, "Incorporating dynamicity of transportation network with multi-weight traffic graph convolutional network for traffic forecasting," *IEEE Trans. Intelligent Transportation Systems*, vol. 23, no. 3, pp. 2082-2092, Mar. 2020, doi: 10.1109/TITS.2020.3031331.
- [32] N. Hu, D. Zhang, K. Xie, W. Liang, and M.Y. Hsieh, "Graph learning-based spatial-temporal graph convolutional neural networks for traffic forecasting," *Connection Science*, vol. 34, no. 1, pp. 429-448, 2022, doi: 10.1080/09540091.2021.2006607.
- [33] Z. Li, G. Xiong, Y. Tian, Y. Lv, Y. Chen, P. Hui, and X. Su, "A multi-stream feature fusion approach for traffic prediction," *IEEE Trans. Intelligent Transportation Systems*, vol. 23, no. 2, pp. 1456-1466, Feb. 2022, doi: 10.1109/TITS.2020.3026836.
- Li Z, Xiong G, Tian Y, Lv Y, Chen Y, Hui P, Su X.
- [34] Z. Pan, Y. Liang, W. Wang, Y. Yu, Y. Zheng, and J. Zhang, "Urban traffic prediction from spatio-temporal data using deep meta learning," in *Proc. 25th ACM SIGKDD Int. Conf. Knowledge Discovery & Data Mining (KDD)*, pp. 1720-1730, 2019, doi: 10.1145/3292500.3330884.
- [35] Z. Wu, S. Pan, G. Long, J. Jiang, X. Chang, and C. Zhang, "Connecting the dots: Multivariate time series forecasting with graph neural networks," in *Proc. 26th ACM SIGKDD Int. Conf. Knowledge Discovery & Data Mining (KDD)*, pp. 753-763, 2020, doi: 10.1145/3394486.3403118.
- [36] W. Zhong, T. Mallick, J. Macfarlane, H. Meidani, P. Balaprakash, "Graph Pyramid Autoformer for Long-Term Traffic Forecasting," in *Proc. IEEE International Conference on Machine Learning and Applications (ICMLA)*, 2023, doi: 10.1109/ICMLA58977.2023.00060.
- [37] W. Zhong, T. Mallick, J. Macfarlane, H. Meidani, P. Balaprakash, "Explainable Graph Pyramid Autoformer for Long-Term Traffic Forecasting," *arXiv preprint arXiv:2209.13123*, 2022.
- [38] T. Bogaerts, A.D. Masegosa, J.S. Angarita-Zapata, E. Onieva, P. Hellinckx, "A graph CNN-LSTM neural network for short and long-term traffic forecasting based on trajectory data," *Transportation Research Part C: Emerging Technologies*, vol. 112, pp. 62-77, 2020, doi: 10.1016/j.trc.2020.01.010.
- [39] J.Q. James, C. Markos, S. Zhang, "Long-term urban traffic speed prediction with deep learning on graphs," *IEEE Transactions on Intel-*

- Intelligent Transportation Systems*, vol. 23, no. 7, pp. 7359-7370, 2022, doi: 10.1109/TITS.2021.3069234.
- [40] D. A. Tedjopurnomo, F. M. Choudhury, and A. K. Qin, "TrafFormer: A Transformer Model for Predicting Long-term Traffic," *arXiv preprint arXiv:2302.12388*, Feb. 2023, doi: 10.48550/arXiv.2302.12388.
- [41] Z. Shao, F. Wang, F. T. Sun, C. Yu, Y. Fang, G. Jin, Z. An, Y. Liu, X. Qu, Y. Xu, "HUTFormer: Hierarchical U-Net Transformer for Long-Term Traffic Forecasting," *arXiv preprint arXiv:2307.14596*, Jul. 2023, doi: 10.48550/arXiv.2307.14596.
- [42] J. Oakley, C. Conlan, G. V. Demirci, A. Sfyridis, H. Ferhatosmanoglu, "Foresight Plus: Serverless Spatio-Temporal Traffic Forecasting," *Geoinformatica*, 2024, doi: 10.1007/s10707-024-00517-9.
- [43] B. Hu, C. Lv, M. Li, Y. Liu, X. Zheng, F. Zhang, W. Cao, and F. Zhang, "SpikeSTAG: Spatial-Temporal Forecasting via GNN-SNN Collaboration," *arXiv preprint arXiv:2508.02069*, 2025.
- [44] Y. Song, R. Luo, T. Zhou, C. Zhou, R. Su, "GAT-Informer: A Graph Attention Informer Model for Traffic Flow Prediction under the Impact of Sports Events," *Sensors*, vol. 24, no. 15, art. no. 4796, 2024, doi: 10.3390/s24154796.
- [45] A. Vaswani, N. Shazeer, N. Parmar, J. Uszkoreit, L. Jones, A. N. Gomez, Ł. Kaiser, and I. Polosukhin, "Attention is all you need," in *Advances in Neural Information Processing Systems (NeurIPS)*, vol. 30, 2017.
- [46] L. Cai, K. Janowicz, G. Mai, B. Yan, and R. Zhu, "Traffic Transformer: Capturing the Continuity and Periodicity of Time Series for Traffic Forecasting," *Transactions in GIS*, vol. 24, no. 3, pp. 736-755, 2020.
- [47] M. Xu, W. Dai, C. Liu, X. Gao, W. Lin, G.-J. Qi, and H. Xiong, "Spatial-Temporal Transformer Networks for Traffic Flow Forecasting," *arXiv:2001.02908*, 2020.
- [48] H. Yan, X. Ma, and Z. Pu, "Learning Dynamic and Hierarchical Traffic Spatiotemporal Features With Transformer," *IEEE Transactions on Intelligent Transportation Systems*, vol. 23, no. 11, pp. 22386-22399, 2022.
- [49] C. Chen, Y. Liu, L. Chen, and C. Zhang, "Bidirectional Spatial-Temporal Adaptive Transformer for Urban Traffic Flow Forecasting," *IEEE Transactions on Neural Networks and Learning Systems*, vol. 34, no. 10, pp. 6913-6925, 2023.
- [50] Y. Wen, P. Xu, Z. Li, W. Xu, and X. Wang, "RPCConvformer: A novel Transformer-based deep neural network for traffic flow prediction," *Expert Systems with Applications*, vol. 218, p. 119587, 2023.
- [51] J. Zhang, J. Jin, J. Tang, and Z. Qu, "FPTN: Fast Pure Transformer Network for Traffic Flow Forecasting," in *ICANN 2023: Artificial Neural Networks and Machine Learning*, vol. 14259, Springer, 2023, pp. 382-393.
- [52] S. Liu and X. Wang, "An improved transformer based traffic flow prediction model," *Scientific Reports*, vol. 15, p. 8284, 2025.
- [53] A. Chang, Y. Ji, and Y. Bie, "Transformer-based short-term traffic forecasting model considering traffic spatiotemporal correlation," *Frontiers in Neuroinformatics*, vol. 19, p. 1527908, 2025.
- [54] J. Ma, J. Zhao, and Y. Hou, "Spatial-Temporal Transformer Networks for Traffic Flow Forecasting Using a Pre-Trained Language Model," *Sensors*, vol. 24, no. 17, p. 5502, 2024.
- [55] Y. Tian, W. Li, X. Wang, X. Yan, and Y. Xu, "Transformer-Based Traffic Flow Prediction Considering Spatio-Temporal Correlations of Bridge Networks (ST-TransNet)," *Applied Sciences*, vol. 15, no. 16, p. 8930, 2025.
- [56] W. Kong, Y. Ju, S. Zhang, J. Wang, L. Huang, H. Qu, "Graph Enhanced Spatial-Temporal Transformer for Traffic Flow Prediction," *Applied Soft Computing*, vol. 170, p. 112698, 2025.
- [57] W. Sun, R. Cheng, Y. Jiao, and J. Gao, "Decoupled Graph Spatial-Temporal Transformer Networks for Traffic Flow Forecasting," *Engineering Applications of Artificial Intelligence*, vol. 148, p. 110476, 2025.
- [58] J. Zhang, Y. Yang, X. Wu, and S. Li, "Spatio-temporal Transformer and Graph Convolutional Networks Based Traffic Flow Prediction," *Scientific Reports*, vol. 15(1), p. 24299, 2025.
- [59] X. He, W. Zhang, X. Li, and X. Zhang, "TEA-GCN: Transformer-Enhanced Adaptive Graph Convolutional Network for Traffic Flow Forecasting," *Sensors*, vol. 24, no. 21, p. 7086, 2024.
- [60] D. Jin, C. Huo, J. Shi, D. He, J. Wei, and P.S. Yu, "LLGformer: Learnable Long-range Graph Transformer for Traffic Flow Prediction," In Proceedings of the ACM on Web Conference, (pp. 2860-2871), 2025.
- [61] Federal Highway Administration (FHWA), "Traffic Incident Management Performance Measures," Office of Operations, U.S. Department of Transportation. [Online]. Available: https://ops.fhwa.dot.gov/tim/preparedness/tim/performance_measures.htm
- [62] R. Li, F. C. Pereira, and M. E. Ben-Akiva, "Overview of traffic incident duration analysis and prediction," *European Transport Research Review*, vol. 10, art. no. 22, May 2018, doi: 10.1186/s12544-018-0300-1.
- [63] H. Korkmaz and M. A. Erturk, "Prediction of the traffic incident duration using statistical and machine-learning methods: A systematic literature review," *Technological Forecasting and Social Change*, art. no. 123621, 2024, doi: 10.1016/j.techfore.2024.123621.
- [64] R. Corbally, L. Yang, and A. Malekjafarian, "Predicting the duration of motorway incidents using machine learning," *European Transport Research Review*, vol. 16, art. no. 14, 2024, doi: 10.1186/s12544-024-00632-6.
- [65] National Center for Statistics and Analysis, National Highway Traffic Safety Administration, "Speeding: 2023 Data," *Traffic Safety Facts Research Note*, DOT HS 813 721.
- [66] Q. Xie, T. Guo, Y. Chen, Y. Xiao, X. Wang, and B. Y. Zhao, "Deep Graph Convolutional Networks for Incident-Driven Traffic Speed Prediction," in *Proc. 29th ACM Int. Conf. on Information and Knowledge Management (CIKM)*, 2020, pp. 1665-1674, doi: 10.1145/3340531.3411873.
- [67] S. Chaudhuri, P. Juan, and J. Mateu, "Spatio-temporal modeling of traffic accidents incidence on urban road networks based on an explicit network triangulation," *Journal of Applied Statistics*, vol. 50, no. 16, pp. 3229-3250, 2023, doi: 10.1080/02664763.2022.2104822.
- [68] J. Jin, P. Liu, H. Huang, and Y. Dong, "Analyzing urban traffic crash patterns through spatio-temporal data: A city-level study using a sparse non-negative matrix factorization model with spatial constraints approach," *Applied Geography*, vol. 172, art. no. 103402, Nov. 2024, doi: 10.1016/j.apgeog.2024.103402.
- [69] P. T. Savolainen, F. L. Mannering, D. Lord, and M. A. Qaddus, "The statistical analysis of highway crash-injury severities: A review and assessment of methodological alternatives," *Accident Analysis & Prevention*, vol. 43, no. 5, pp. 1666-1676, 2011, doi: 10.1016/j.aap.2011.03.025.
- [70] P. Penmetsa and S. S. Pulugurtha, "Modeling crash injury severity by road feature to improve safety," *Traffic Injury Prevention*, vol. 19, no. 1, pp. 102-109, 2018, doi: 10.1080/15389588.2017.1335396.
- [71] A. Jamal, M. Zahid, M. T. Rahman, H. M. Al-Ahmadi, M. Almoshaogeh, D. Farooq, and M. Ahmad, "Injury severity prediction of traffic crashes with ensemble machine learning techniques: a comparative study," *International Journal of Injury Control and Safety Promotion*, vol. 28, no. 4, pp. 408-427, 2021, doi: 10.1080/17457300.2021.1928233.
- [72] X. Yan, J. He, C. Zhang, Z. Liu, C. Wang, and B. Qiao, "Spatiotemporal instability analysis considering unobserved heterogeneity of crash-injury severities in adverse weather," *Analytic Methods in Accident Research*, vol. 32, art. no. 100182, 2021, doi: 10.1016/j.amar.2021.100182.
- [73] Y. Wu and J. J. Q. Yu, "A Bayesian learning network for traffic speed forecasting with uncertainty quantification," in *Proc. Int. Joint Conf. Neural Networks (IJCNN)*, 2021, pp. 1-7.
- [74] Y. Gal and Z. Ghahramani, "Dropout as a Bayesian approximation: Representing model uncertainty in deep learning," in *Proc. 33rd Int. Conf. Mach. Learn. (ICML)*, PMLR, vol. 48, 2016, pp. 1050-1059.
- [75] B. Lakshminarayanan, A. Pritzel, and C. Blundell, "Simple and scalable predictive uncertainty estimation using deep ensembles," in *Advances in Neural Information Processing Systems*, vol. 30, 2017, pp. 6402-6413.
- [76] K. Stankevičiūtė, A. Alaa, and M. van der Schaar, "Conformal time-series forecasting," in *Advances in Neural Information Processing Systems*, vol. 34, 2021, pp. 11334-11344.
- [77] Y. Romano, E. Patterson, and E. J. Candès, "Conformalized quantile regression," in *Advances in Neural Information Processing Systems*, vol. 32, 2019, pp. 3538-3548.
- [78] I. Gibbs and E. J. Candès, "Adaptive conformal inference under distribution shift," in *Advances in Neural Information Processing Systems*, vol. 34, 2021, pp. 1660-1672.
- [79] M. Zaffran, O. Féron, Y. Goude, J. Josse, and A. Dieuleveut, "Adaptive conformal predictions for time series," in *Proc. 39th Int. Conf. Mach. Learn. (ICML)*, PMLR, vol. 162, 2022, pp. 25834-25866.
- [80] Y. Nie, N. H. Nguyen, P. Sinthong, and J. Kalagnanam, "A Time Series is Worth 64 Words: Long-term Forecasting with Transformers," in *Proc. Int. Conf. on Learning Representations (ICLR)*, 2023.
- [81] J. Liu and W. Guan, "A summary of traffic flow forecasting methods," *Journal of Highway and Transportation Research and Development*, 2004.
- [82] B. M. Williams and L. A. Hoel, "Modeling and forecasting vehicular traffic flow as a seasonal ARIMA process: Theoretical basis and empirical results," *Journal of Transportation Engineering*, vol. 129, no. 6, pp. 664-672, 2003.
- [83] Y. Xie, K. Zhao, Y. Sun, and D. Chen, "Gaussian processes for short-term traffic volume forecasting," *Transportation Research Record*, vol. 2165, no. 1, pp. 69-78, 2010.
- [84] D. A. Nix and A. S. Weigend, "Estimating the mean and variance of the target probability distribution," in *Proc. 1994 IEEE Int. Conf. Neural Networks (ICNN'94)*, vol. 1, pp. 55-60, 1994.

- [85] A. J. Khattak, J. Liu, B. Wali, X. Li, and M. Ng, "Modeling traffic incident duration using quantile regression," *Transportation Research Record*, vol. 2554, no. 1, pp. 139-148, 2016.
- [86] A. Matas, J.-L. Raymond, and A. Ruiz, "Traffic forecasts under uncertainty and capacity constraints," *Transportation*, vol. 39, pp. 1-17, 2012.
- [87] M. Patil, P. Tulpule, and S. Midlam-Mohler, "An approach to model a traffic environment by addressing sparsity in vehicle count data," SAE Technical Paper 2023-01-0854, 2023.
- [88] Y. Gal and Z. Ghahramani, "Dropout as a Bayesian approximation: Representing model uncertainty in deep learning," in *Proc. Int. Conf. Mach. Learn. (ICML)*, PMLR, 2016, pp. 1050-1059.